



UNIVERSITÉ PAUL SABATIER



PROJECT ERASMUS

Characterization of a dielectric barrier discharge

Fábio Romero Brito Monteiro

15/07/2013

Mr NeermalsingVassantSewraj
Mr George Zisis
Mr Carlos Torres

Tutor UPS
Coordinator UPS
Coordinator UNICAN

Thanks

I would like to thank all the personnel of the laboratory LAPLACE that directly or indirectly contributed to my work.

Especially I would like to express my thanks to Mr Neermalsing Vasant Sewraj, my tutor. It's really rewarding to work with a person who enjoys his job.

I dedicate this project to all my family especially my parents, sister and Mr Pedro Romero Brito Monteiro.

I also dedicate this project to family Kets, especially Jill Kets that with her support helped me to achieve my goals.

Index

Thanks	2
Introduction	5
Objective	6
Sinusoidal-Mode	7
Experimental Setup.....	7
Current and aspect of the discharge.....	8
Current-voltage characteristic of the microdischarge	9
Description of the evolution of the discharge	10
Temporal evolution of voltage.....	11
Temporal evolution of current.....	12
Influence of pressure on current wave forms	13
Influence of distance on current wave forms	14
Study of mono-filament micro-discharge in pure xenon.....	14
Ignition voltage (onset voltage)	14
Energy injected into one microdischarge	15
The instantaneous power deposited in the plasma	16
Study of mono-filament micro-discharge in synthetic air	17
Ignition voltage (onset voltage)	17
Energy injected into one microdischarge	18
Pulse-Mode	20
Pulse Generator	20
Experimental Setup.....	21
Brief description of its main features and changes	21
Electrical Circuit	22
Temporal expressions and medium currents and voltages	22
Temporal expressions and medium power	22
Study of the circuit behaviour.....	23
Voltage and current wave forms	25
Characteristic of the microdischarge	26
DBD-establishment for 3 mm gap at 400 Torr.....	28
Temporal evolution of current.....	31
Energy into one microdischarge	31
Pressure influence.....	32

Distance influence.....	32
Ignition voltage	32
Pressure influence.....	33
Distance influence.....	33
Matlab.....	34
Objective:	34
Operating description	34
Difficulties	34
Interpretation of results.....	34
Calculation of capacitor C_p	34
Voltage rise time	35
Application	36
Ethylene elimination.....	36
New photocatalytic process	37
Experimental Setup.....	37
Operating description of the photocatalytic reactor	37
Conclusion.....	38
Bibliography	39

Introduction

Dielectric barrier discharge (DBDs) have been studied since 1857. For the past three decades, DBDs have been considerably developed for the realization of ultraviolet (UV) and vuv radiation sources.

These radiation sources seem very promising for discharges operating in rare gases or rare gas/halogen.

Dielectric barrier discharges (DBDs) are widely used in industrial applications, such as pollution control, decontamination or sterilization, material deposition, surface treatment, vacuum ultraviolet (VUV) as well as light sources. During the last decade, various research investigations in plasma and medical fields have also been initiated, namely wound healing, blood coagulation and homeostasis, as well as malignant cell inactivation.

The intent of this project is to perform an experimental analysis of the dielectric barrier discharge with the different behavior for different pressure, distance. We also analyzed different types of gas (Xenon and Synthetic air).

Xenon based dielectric barrier discharges (DBDs) are very famous for industrial purposes, due to their high efficiency in converting electrical energy into intense and sharp emission of the unabsorbed molecular Xe 2nd continuum at 172 nm.

We also analyzed the behavior with different kinds of source, sinusoidal and pulse.

This work study in more depth the influence of pulse-mode. According to some authors, the short-pulse mode is much more efficient than the sine-mode. So, monopolar voltage pulses can be a good means to further enhance the electrical to VUV energy conversion of Xe DBDs. However, this may be achieved to the detriment of the absolute electrical input power.

For a real application there are others study that isn't mentioned here, for example the produce of VUV for the different types of gas, the influence of the frequency, ect.

This study will help to know what the best pressure and distance and gas for each type of application.

Objective

- Influence of the pressure, distance and gas
- Analysis of the different behavior pulse-mode, sinusoidal-mode.
- A better understanding of the influence of the pulsed mode.
- Seek for the best excitation mode for optimal emissions of DBDs
- Validation of 2D numerical code meant for modelling of Xe MF-DBDs

Sinusoidal-Mode

Experimental Setup

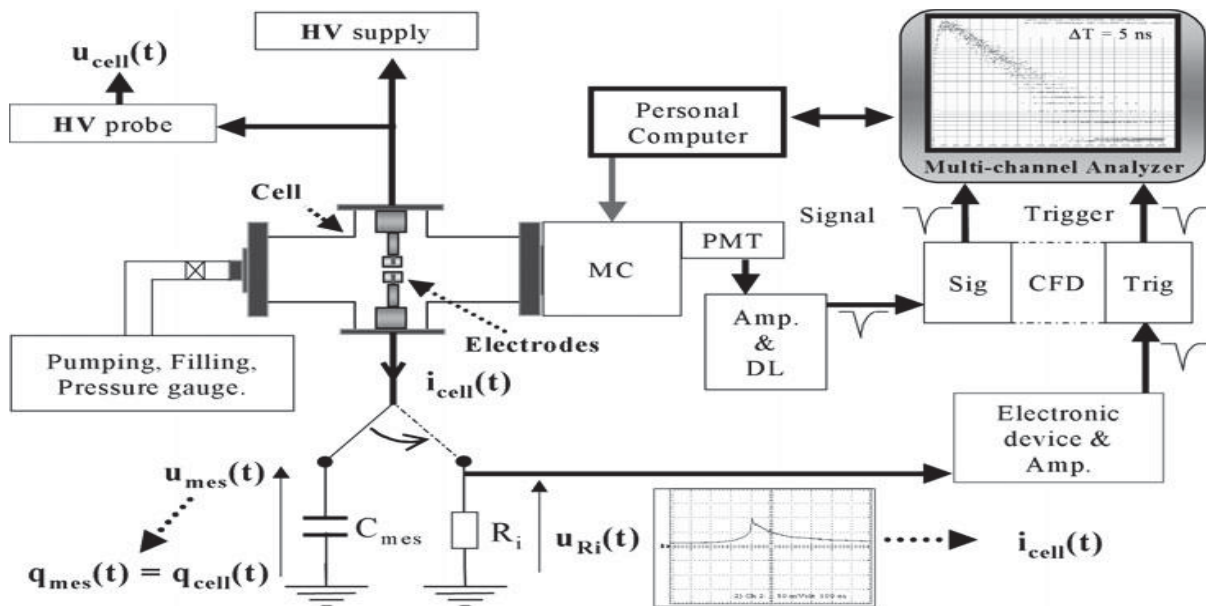


Fig. 1 : Experimental setup

Reference: Laboratory LAPLACE

1. Cell

Cylindrical glass, where it creates the necessary conditions for the study of the microdischarge.

2. Electrodes

It is important for our study only one microdischarge is obtained at a time, and that be as stable as possible. Because of that are used small dimensions of the electrodes.

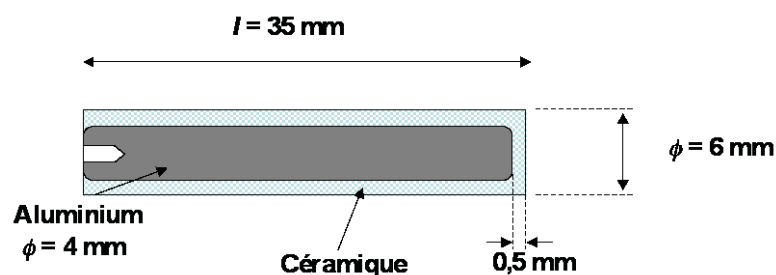


Fig. 2: Electrodes

Reference: Laboratory LAPLACE

3. Gas used

The discharges were carried out in a pure rare gas, in the case of xenon, and in a pure gas in the case of the synthetic air.

4. Bench pumping

Responsible for maintaining the gas purity, in order to avoid the transfer of energy through the impurities.

Current and aspect of the discharge

The Fig.3 represents the voltage applied u_{cell} the electrodes and the current i_{cell} that through the cell for a pressure $P_{\text{xe}}=500\text{Torr}$, a frequency $f=10\text{kHz}$, and a distance $d=2\text{mm}$.

There are two components can be distinguished in the current:

- A weak current sinusoidal due to the movement of charges on the dielectric layers.
- A current pulse whose duration depends on the pressure.

For all xenon pressures, wave forms of the cell current were quite similar, differing only by the values of their rise times, pulse durations, and maxima.

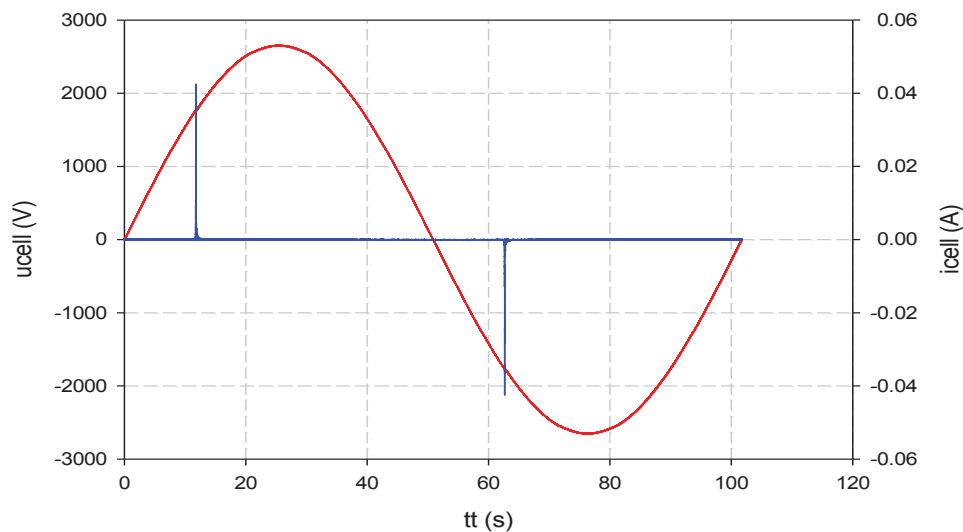


Fig. 3: $P_{\text{xe}}=400\text{Torr}$, $f=10\text{kHz}$, $d=2\text{mm}$, $U_{\text{max}}= 2.652\text{ kV}$

The comparison of the two semi period successive show, on the one hand, the inversion anode-cathode, and secondly, the symmetry of the sinusoidal phenomenon.

Current-voltage characteristic of the microdischarge

The characteristic of the micro-discharge in the xenon, obtained from the calculated quantities of $i_{\text{dis}}(t)$ and $u_{\text{dis}}(t)$, which is depicted in Fig. 4, for $P_{\text{Xe}}=400$ Torr, $f=10$ kHz.

We distinguish the phase of the initial electronic avalanche where the discharge current $i_{\text{dis}}(t)$ increased with constant voltage $u_{\text{dis}}(t)$, then phase stream in which the current increased but the voltage decreased. We can also distinguish the phase of the excitation current in which the current and voltage decrease until the extinction of the discharge.

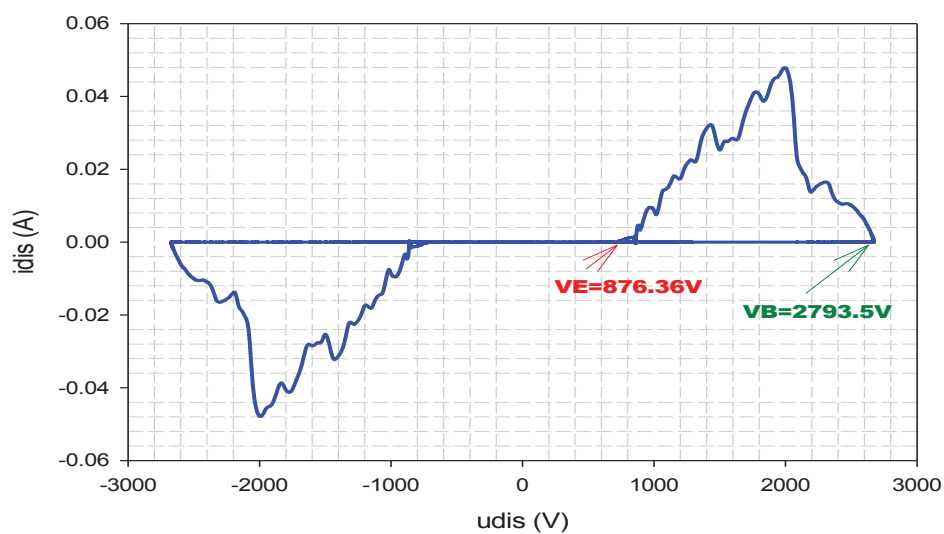


Fig 4: $P_{\text{Xe}}=400$ Torr, $f=10$ kHz, $d=2$ mm, $U_{\text{max}}= 2.6527$ kV

Description of the evolution of the discharge

- 1- The gas ignition when u_{dis} reaches V_B .

Prior to discharge, the voltage u_{cell} across the cell and the voltage u_{dis} applied to the gas increase until the electric field is sufficient to initiate an avalanche. This particular value of the voltage is called the gas ignition voltage V_B .

- 2- The electronic avalanche phase during which i_{dis} increases while u_{dis} remains constant.

The ionization leads to the development of electron avalanche which propagates towards the anode. As the ion mobility is much less than that of the electrons (around 1000 times lower), because the ion is much heavier than the electron, the electron accelerated with greater velocity toward the anode. They leave behind almost immobile ions positives.

When the ionization wave hits the anode the charge are deposited on the surface of the anode, causing a local reduction of the axial electric field. In this instant the current decreases.

- 3- The cathode directed streamer phase during which i_{dis} increases (due to cathode layer formation) while u_{dis} decreases (due to charge accumulation).

There are the creations of new electrons to the rear of the avalanche. During the initial avalanche, the photoelectrons generated near the cathode are accelerated by the local field, and cause secondary avalanches. Fast electrons produced, move to the area of positive space charge, leaving behind positive ions. The result is an apparent displacement of positive charges to the cathode, creating a conductive channel. This is why the discharge current and i_{cell} grow again.

- 4- The extinguishing phase during which both i_{dis} and u_{dis} decrease (due to charge accumulation).

The current increases until reaches its maximum. The charges which accumulate on dielectric surfaces induce an electric field that opposes the applied field. The axial electric field in the gas tends to decrease, this leads to a decrease the speed of current rise.

- 5- The complete extinction of discharge when u_{dis} is equal to V_E .

The extinction of the discharge starts on the side of the anode. This can be explained by the reduction of local axial field side of the anode due to charges accumulated on the surface.

Temporal evolution of voltage

The Fig. 5 gives the temporal evolution of the applied voltage, u_{cell} , the current flowing through the cell, i_{cell} and the voltages u_{die} and u_{dis} , for a pressure of xenon $P_{\text{Xe}}=400$ Torr, $d=2\text{mm}$ and a frequency $f=10\text{kHz}$, where u_{cell} and i_{cell} are the electrical quantities measured, while the other electrical quantities are calculated from a electrical model.

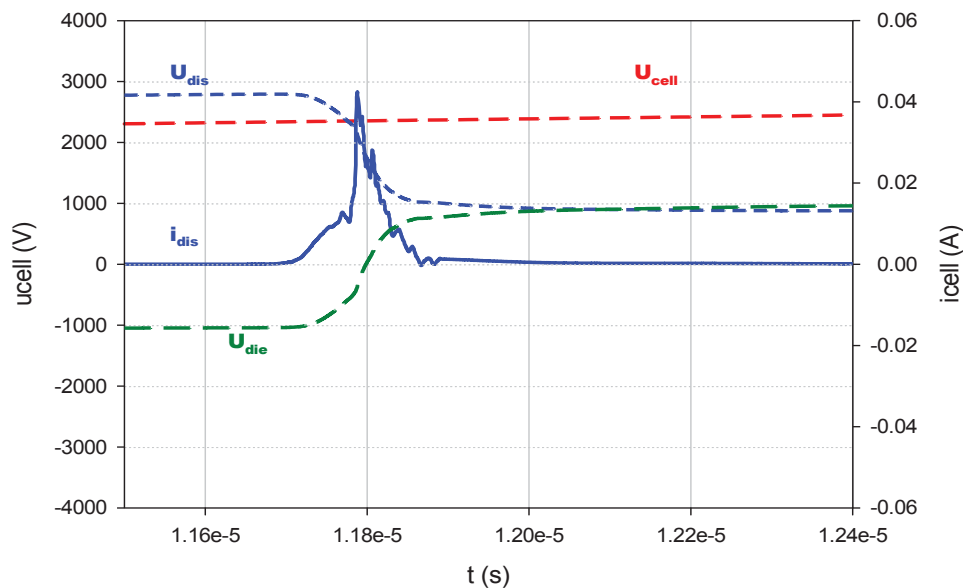


Fig 5: $P_{\text{Xe}}=400$ Torr, $f=10$ kHz, $d=2\text{mm}$

U_{die} starts with a negative value due to the charge accumulated on the dielectric layers during the previous negative half-cycle. U_{dis} rises until it reaches the ignition voltage $V_B=2793.5\text{V}$ (Fig4), when ignition occurs. During the microdischarge, which lasts for 25 ns, the gap voltage decreases due to charge accumulation on the dielectric layers, whereas the supply voltage u_{cell} hardly varies. The discharge fades out when the gap voltage falls to $V_E=876.36$ V (Fig4), the extinction voltage.

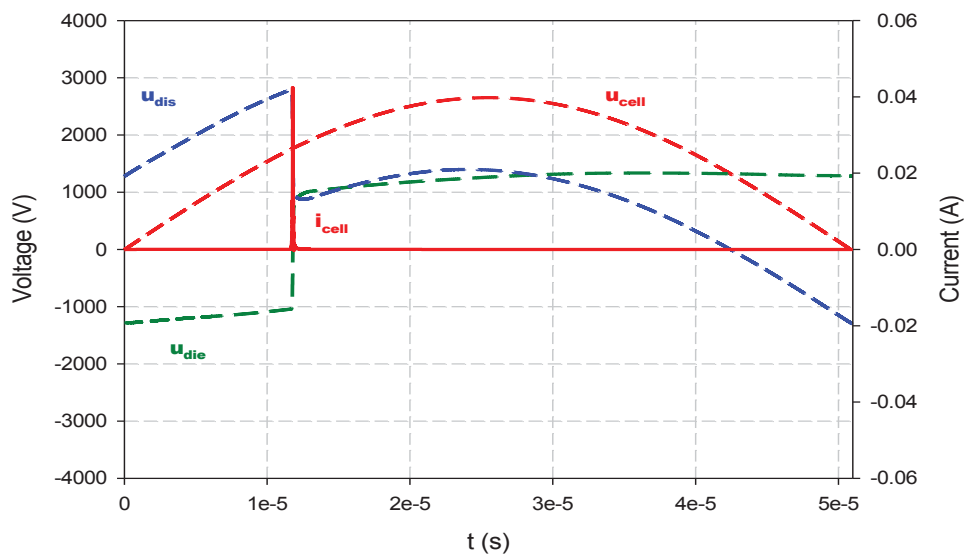


Fig 5: $P=400$ Torr, $f=10\text{kHz}$, $d=2\text{mm}$

Temporal evolution of current

The three currents i_{cell} , i_{dis} , and i_{gap} (the current flowing through C_{gap}) together with the discharge voltage u_{dis} are given in Fig. 6, with an expanded scale. There is the existence avalanche on the anode. The voltage u_{dis} is constant during the initial avalanche, this is consistent with a breakdown type Townsend.

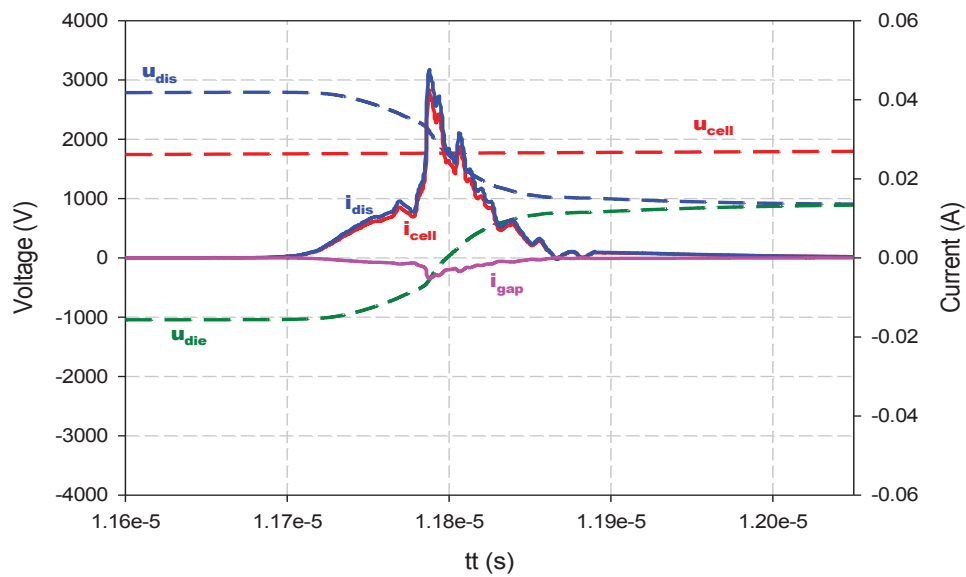


Fig 6: $P_{\text{Xe}}=400$ Torr, $f=10\text{kHz}$, $d=2\text{mm}$

The current discharge, i_{dis} , is greater than the measured one i_{cell} , because, during the discharge phase, the gap voltage decreases continuously.

$$i_{dis} = i_{cell} - i_{gap}$$

$$i_{dis} = \left(1 + \frac{C_{gap}}{C_{die}} \right) * i_{cell} - C_{gap} * \frac{du_{cell}}{dt}$$

Influence of pressure on current wave forms

The maximum current increases with pressure, Fig. 6. The rise time of the current is a function of the pressure.

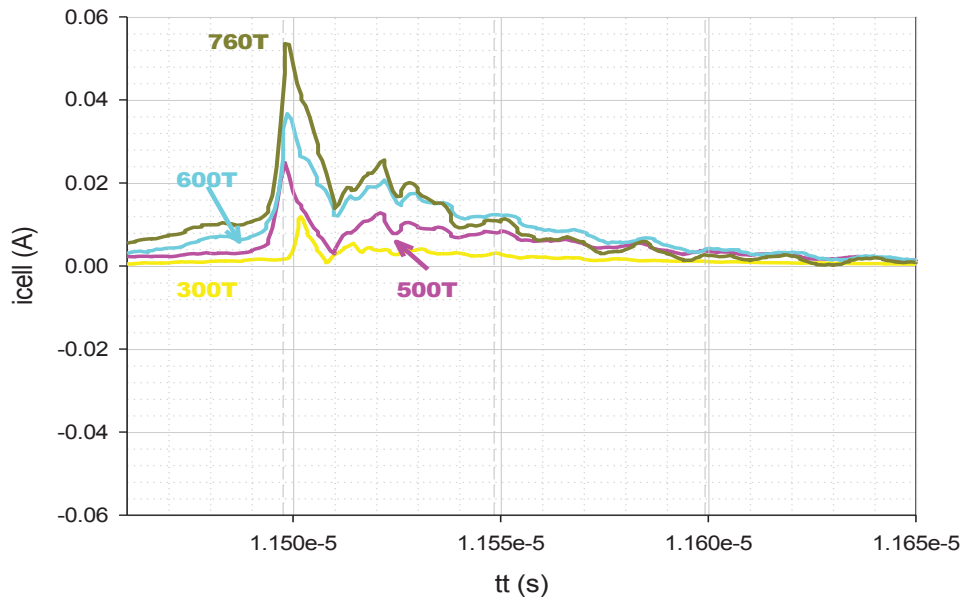


Fig 7: Variable pressure, $d=2mm$, $f=10kHz$

Influence of distance on current wave forms

The maximum current increases with the distance, Fig. 8. The rise time of the current is a function of the distance.

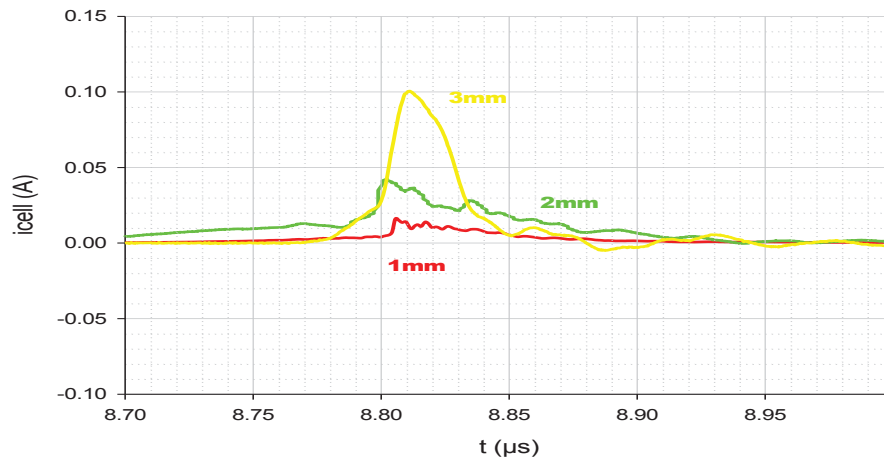


Fig 8: $P=400$ Torr, $f=10\text{kHz}$, variable distance

Study of mono-filament micro-discharge in pure xenon

Ignition voltage (onset voltage)

The ignition voltage (apparent breakdown voltage) V_B , which corresponds to the maximum value of the interelectrode gap voltage u_{dis} .

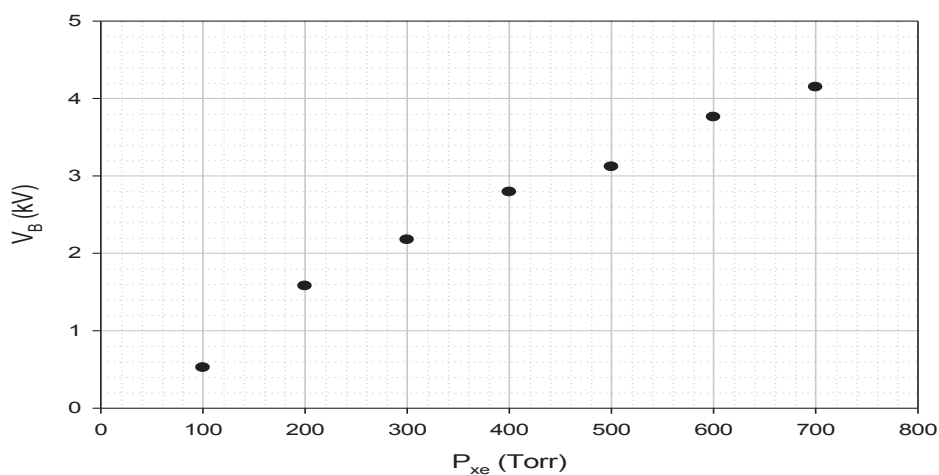


Fig 9: Variable pressure $d=2\text{mm}$

When the pressure increases the ignition voltage increase.

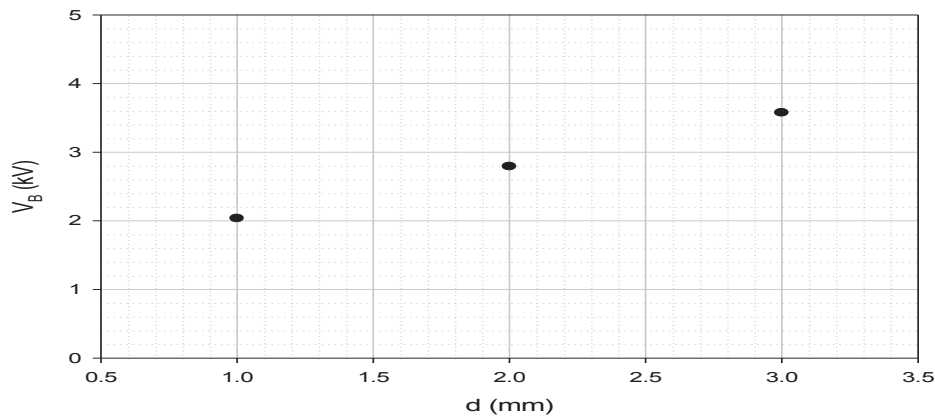


Fig 10: distance variable 400T

When the gap increase need more voltage too beginning the discharge (ignition voltage).

Energy injected into one microdischarge

Fig. 11 shows the almost linear relation between the injected electrical energy, E_{dis} , and the xenon pressure, at a frequency of 10 kHz. This input energy increases with xenon pressure in accordance with higher values of both the cell current and the apparent breakdown voltage.

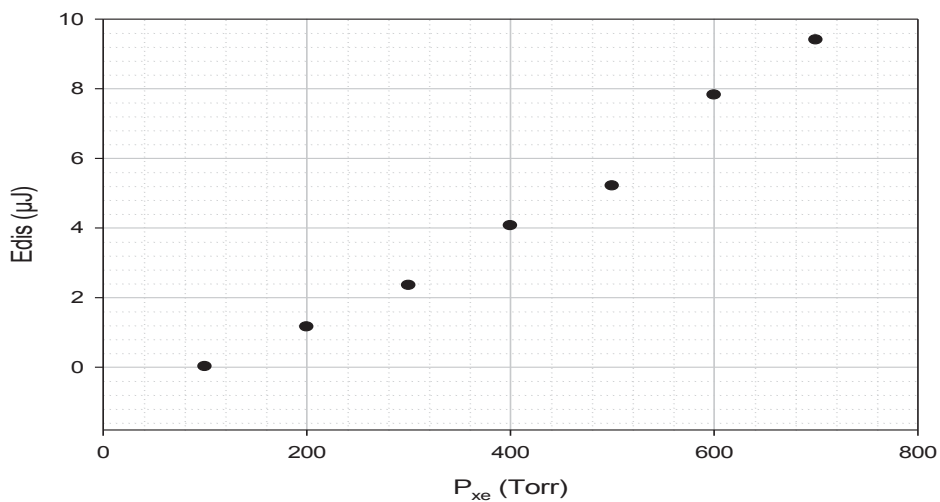


Fig 11: variable pressure d=2mm

Fig. 12 shows the relation between the injected electrical energy, E_{dis} , and the distance. When increase the distance is necessary inject more energy to achieve the gas ignition.

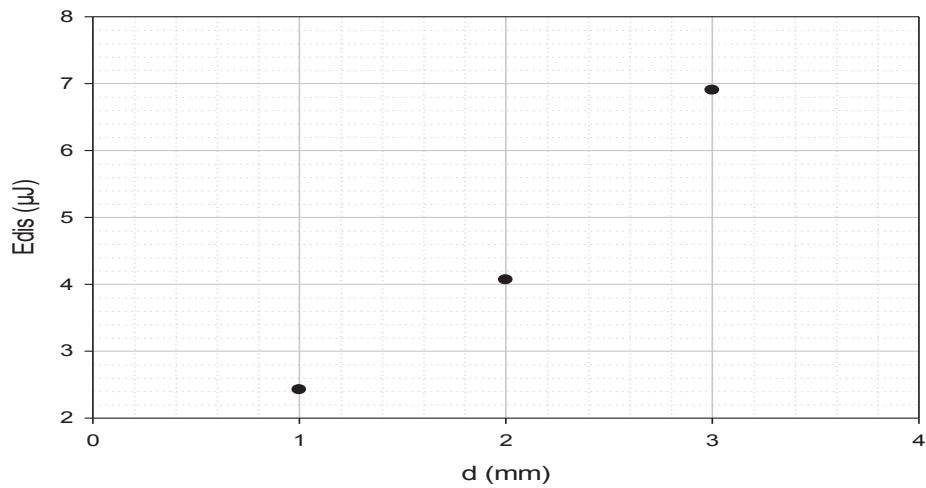


Fig 12: variable distance $P=400$ Torr

The instantaneous power deposited in the plasma

The Fig. 13 shows that higher the pressure the greater the power, this was expected as we had also shown that greater pressure higher current, consequently higher power.

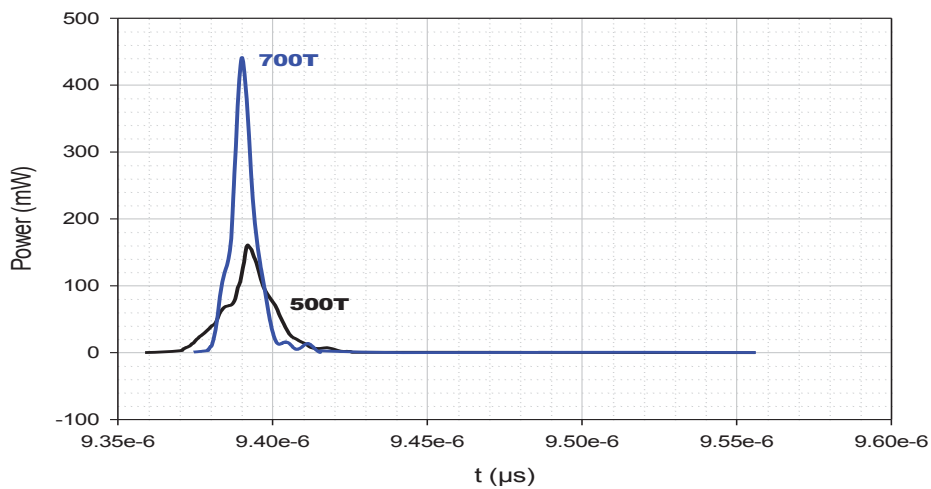


Fig 13: Variable pressure, $d=2$ mm, $f=10$ kHz

Study of mono-filament micro-discharge in synthetic air

Is possible verify that it is much harder to achieve ignition voltage (V_B) in synthetic air than the xenon Fig. 14 this is because of the xenon has impurity and the synthetic air no. This impurity helps the electrons to pass from the valence band to the conduction band.

However once u_{cell} reach V_B we see that the injected electrical energy (E_{dis}) is higher in the synthetic air than the xenon, Fig. 15.

Ignition voltage (onset voltage)

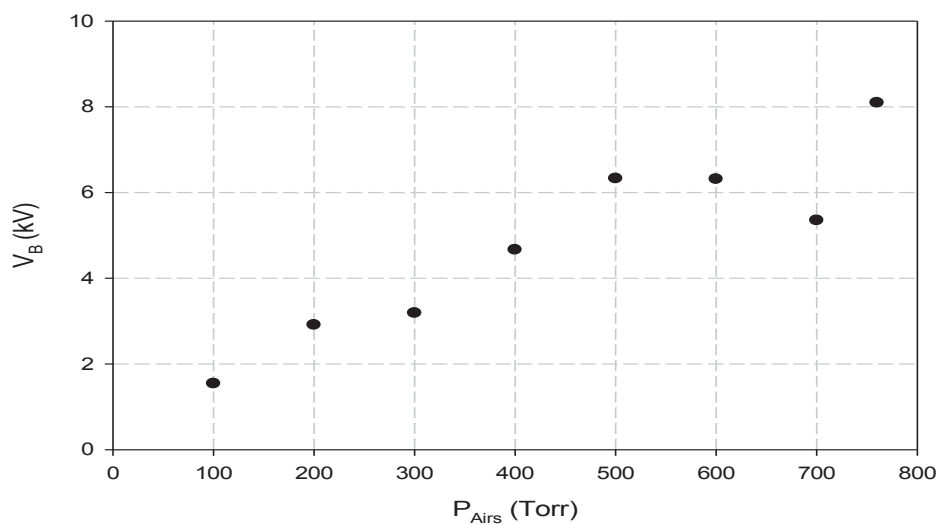


Fig 14: Variable pressure, $f=10\text{kHz}$, $d=1\text{mm}$

In the same way that the xenon, when increase the pressure increase V_B , is possible verify that, in this case, V_B is higher than the observed than xenon.

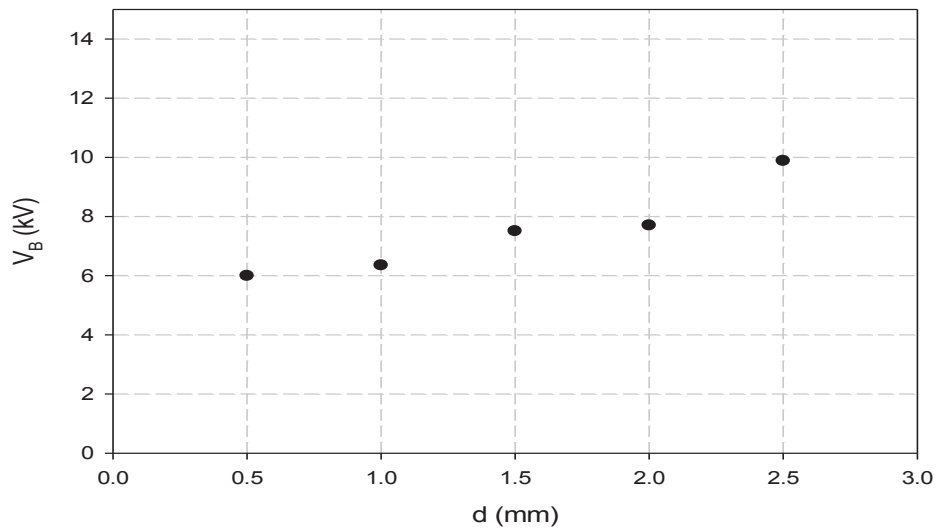


Fig 15: Variable distance, $P=760$ Torr, $f=10$ kHz

As was expected when increase the distance increase V_B .

Energy injected into one microdischarge

As expected, higher values of both the cell current and the apparent breakdown voltage generated an input energy increases, Fig. 16.

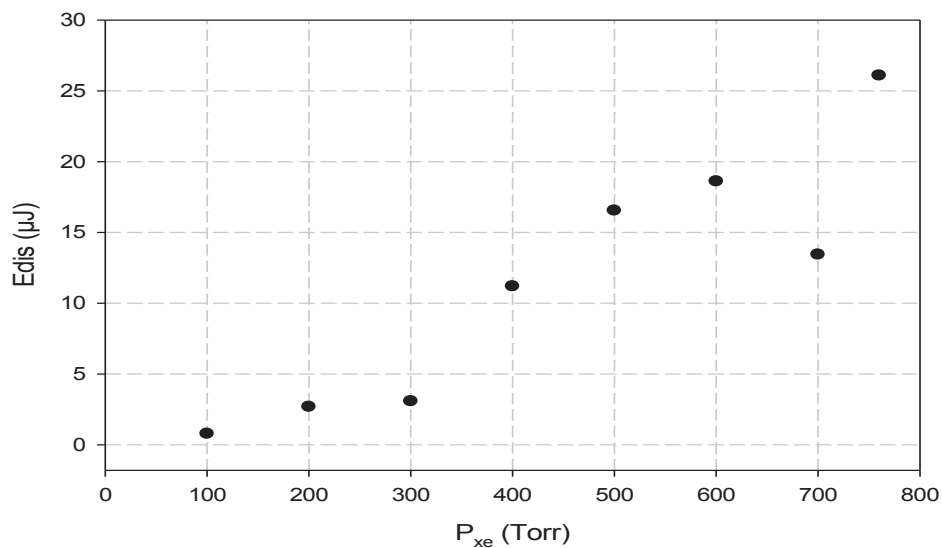


Fig 16: Variable pressure, $d=1$ mm, $f=10$ kHz

When increase the pressure increase E_{dis} .

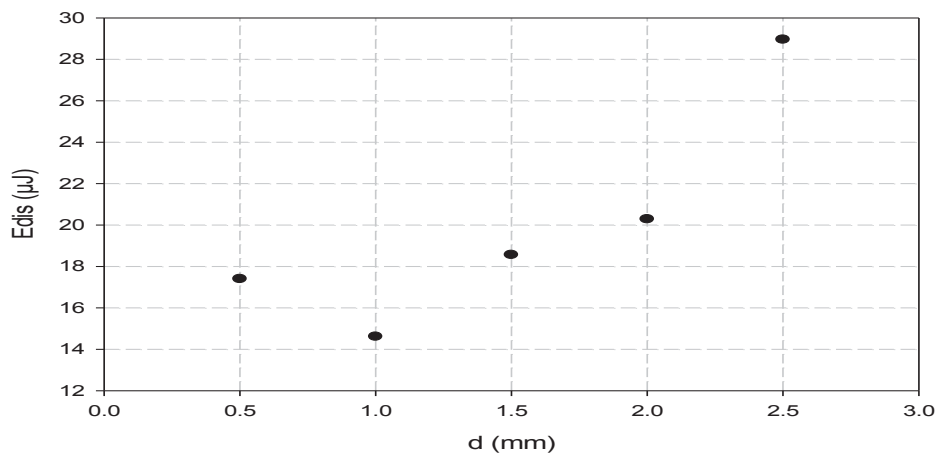


Fig 17: Variable distance, $P=760$ Torr, $f=10$ kHz

When increase the distance increase E_{dis} .

Pulse-Mode

Pulse Generator

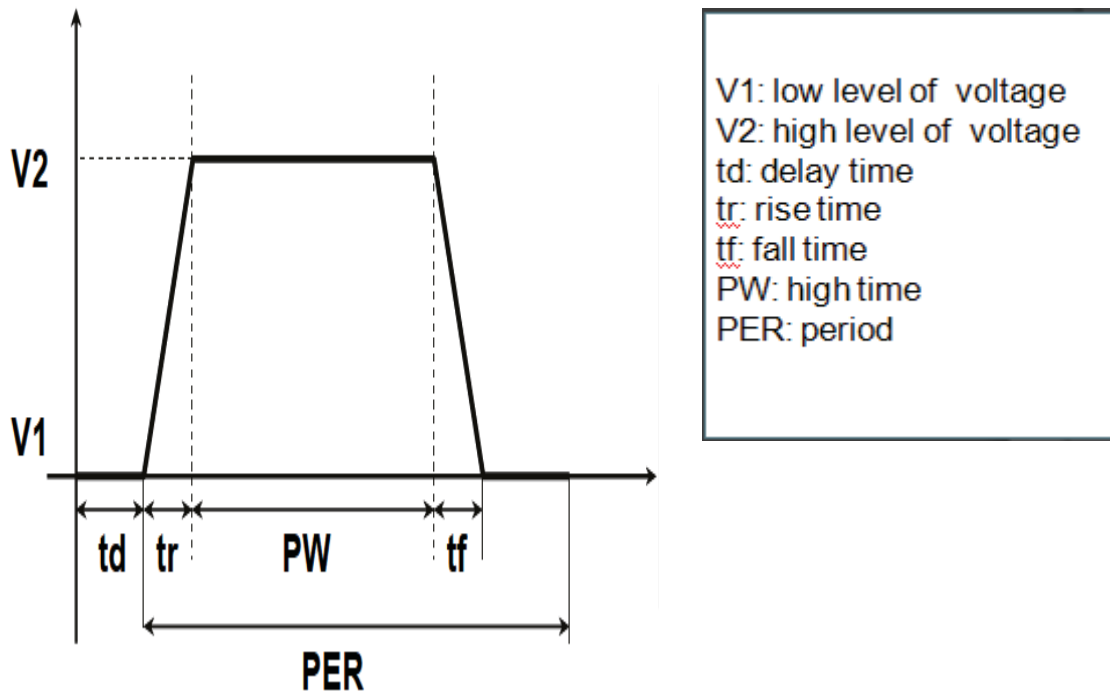


Fig. 18: Pulse generator

Reference: Industrial Electronic (Universidad de Cantabria)

The pulse generator (PVX-4110 DEI) which has the following parameters:

$V_1 = 0 \text{ V}$

$V_2 = \text{Adjustable}$

$t_d = 0 \text{ s}$

$t_r < 60 \text{ ns}$

$t_f < 60 \text{ ns}$

$PW(\tau) = \text{Adjustable}$

$PER = \frac{1}{9.69 \cdot 10^3} = 103.199 \mu\text{s}$

Experimental Setup

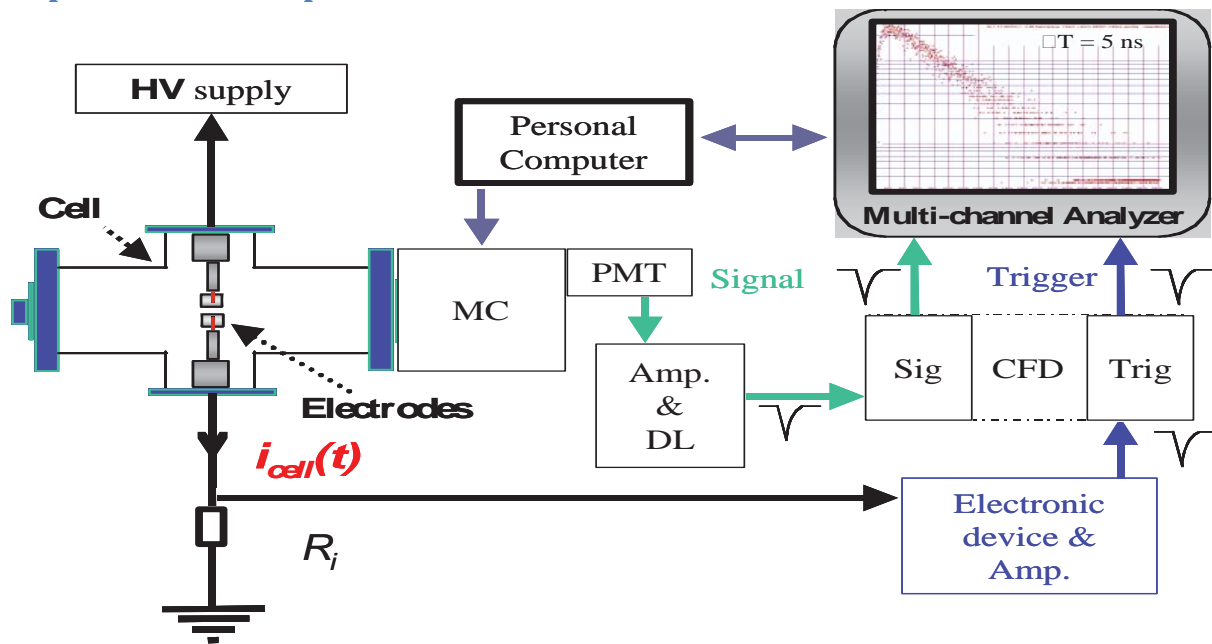


Fig. 19: Experimental setup pulse-mode

Reference: Laboratory LAPLACE

Brief description of its main features and changes

The discharges are achieved in a DBD cell across two identical 4-mm-diameter flat-ended metallic electrodes recovered with 0.5-mm-thick Makor dielectric. One of the electrodes is mounted on a z-translation device in order to perform measurements for different gap distances d .

Mono-polar voltage pulses are generated by means of a PVX-4110 inverter associated to a high voltage TECNİK150-1500 J/s Series DC supply, and driven by a TTL device (PDG-2520). The pulse repetition rate is maintained around $p.r.r. = 9710$ pulses.s⁻¹. Both pulse- amplitude V_M and duration τ are adjustable. To ensure stable and non-diffused discharges for all situations, the rise-time t_{vr} is set to its shortest possible value between 14 and 30 ns, and τ is adjusted accordingly ($125\text{ns} < \tau < 400\text{ns}$).

In order to perform a reproducible and reliable kinetic study of the MF-DBD, N5.0 grade xenon is used, and prior to filling-up at the required pressure P_{Xe} through an aluminium-zirconium getter pump which removes the residual N₂ and O₂ impurities, the bench is pumped down to $\sim 10^{-7}$ Torr.

The supply voltage u_{cell} is recorded with a 500 MHz bandwidth numerical oscilloscope via a high voltage probe. The supply current i_{cell} is obtained with the voltage drop across an adapted 50- Ω series resistance.

Successive snapshots are obtained every 2 ns, and each one corresponds to the accumulation of 100 micro-discharges with 2-ns exposure time. The acquisition time are 1000 ns, much less than the interval separating successive pulses. The TTL signal which drives the fast electronic switches of the inverter is also used to trigger the ICCD camera. Much attention has been paid to reduce jittering.

Electrical Circuit

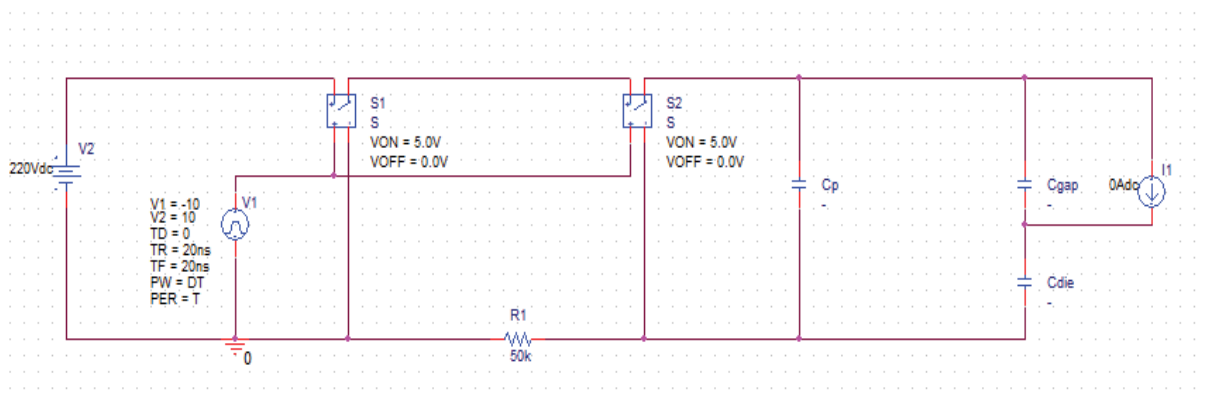


Fig. 20: Electrical Circuit

Temporal expressions and medium currents and voltages

$$u_{\text{cell}}(t) = u_{\text{dis}}(t) + u_{\text{die}}(t)$$

$$i_{\text{cell}}(t) = i_{\text{dis}}(t) + i_{\text{gap}}(t)$$

$$i_{\text{gap}}(t) = C_{\text{gap}} * \frac{du_{\text{dis}}}{dt}$$

$$i_{\text{cell}}(t) = C_{\text{die}} * \frac{du_{\text{die}}}{dt}$$

Operating the above equations

$$i_{\text{dis}}(t) = 1 + \frac{C_{\text{gap}}}{C_{\text{die}}} * i_{\text{cell}}(t) - C_{\text{gap}} * \frac{du_{\text{cell}}}{dt}$$

Temporal expressions and medium power

$$p_{\text{dis}} = u_{\text{dis}}(t) * i_{\text{dis}}(t)$$

$$E_{\text{dis}} = \frac{\langle P_{\text{dis}} \rangle}{2f}$$

Study of the circuit behavior

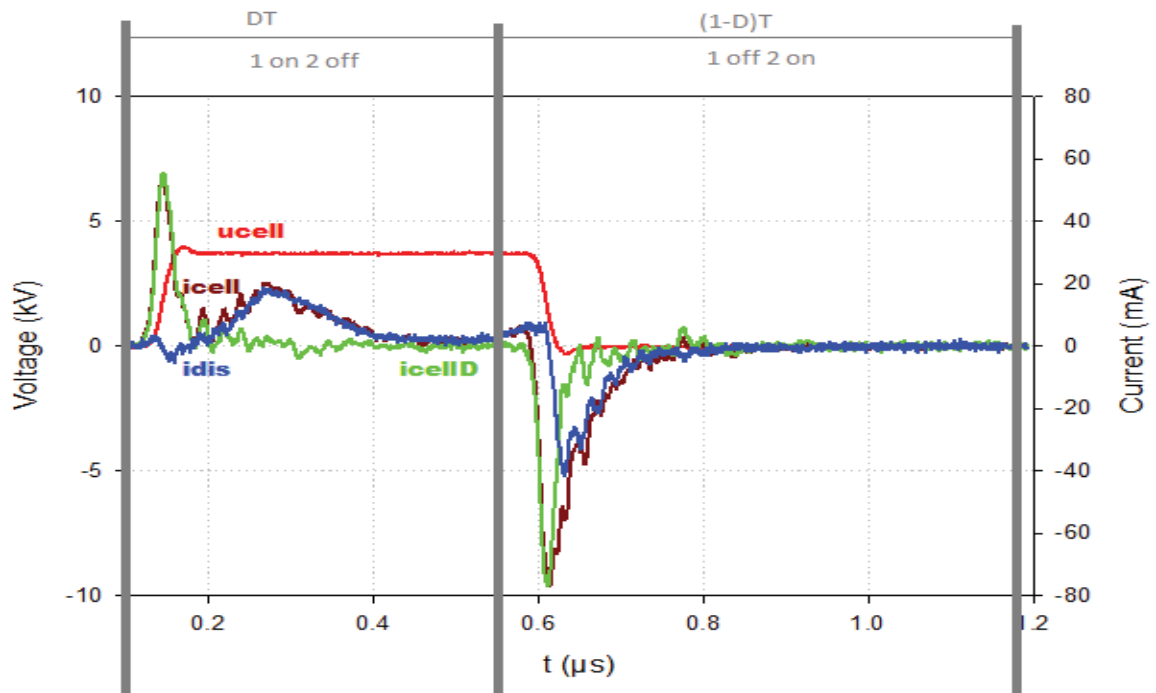
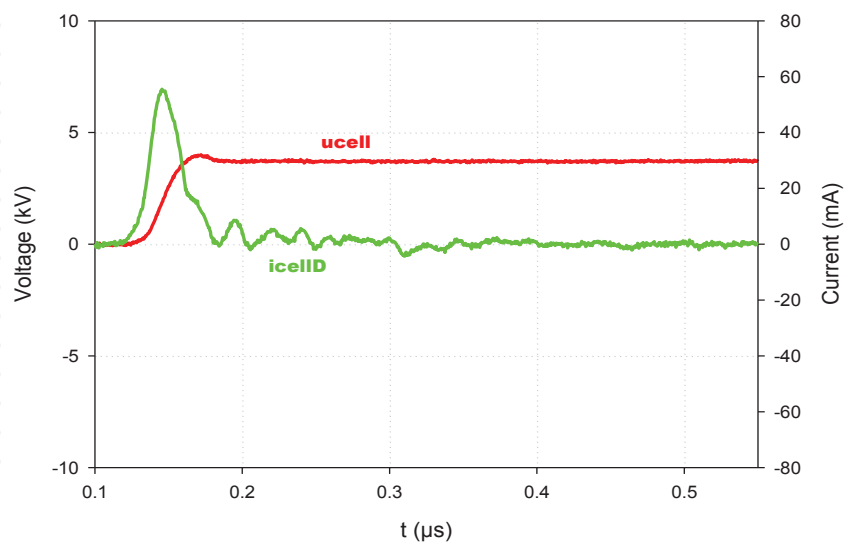
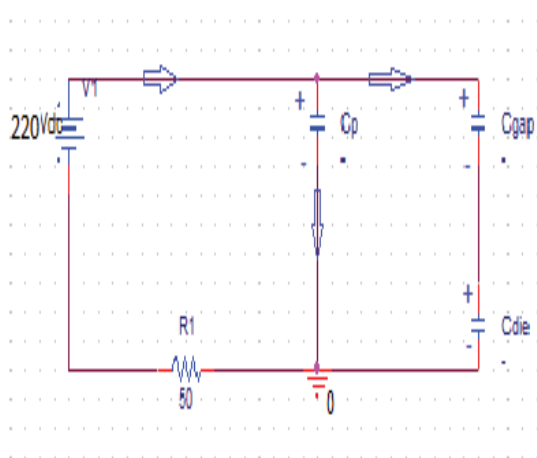


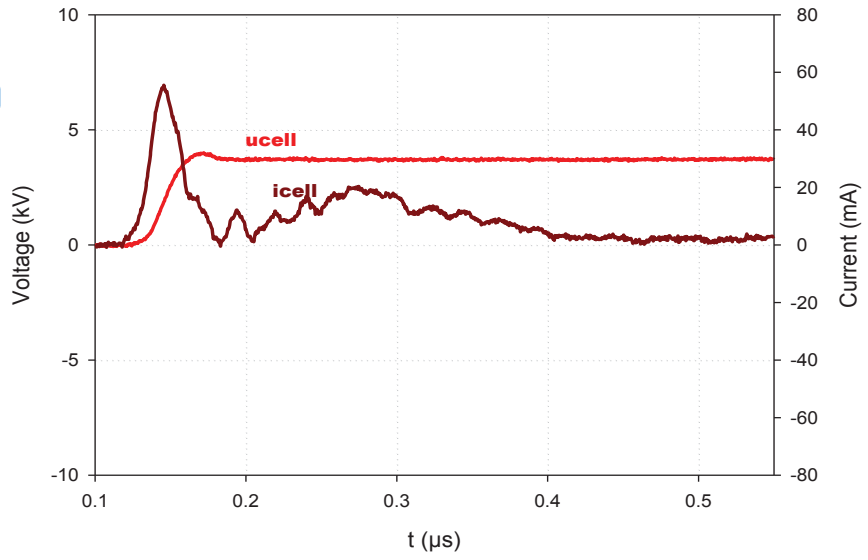
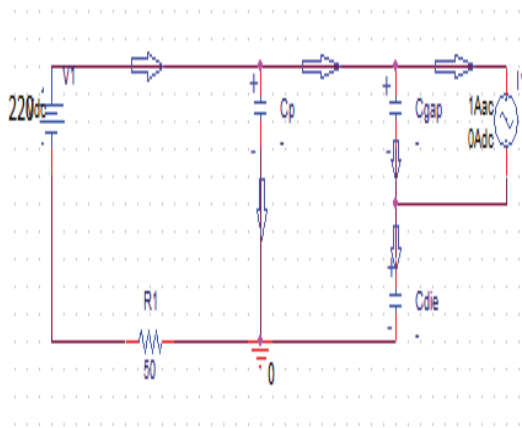
Fig. 21: Analysis of the circuit

It is possible to analyze the influence of the discharge in detail.

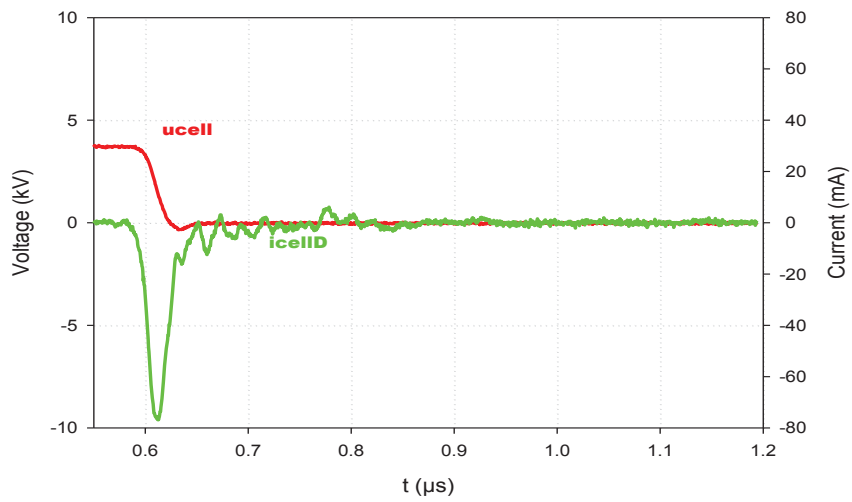
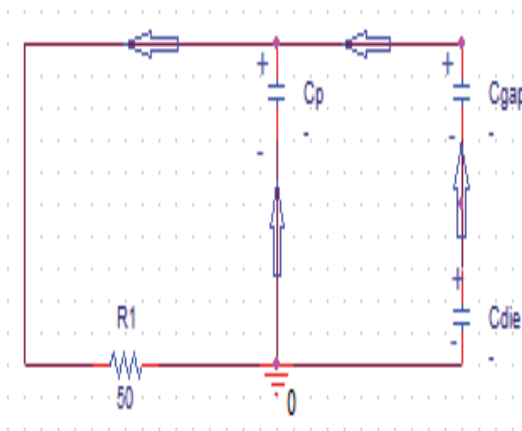
1 on 2 off (without discharge)



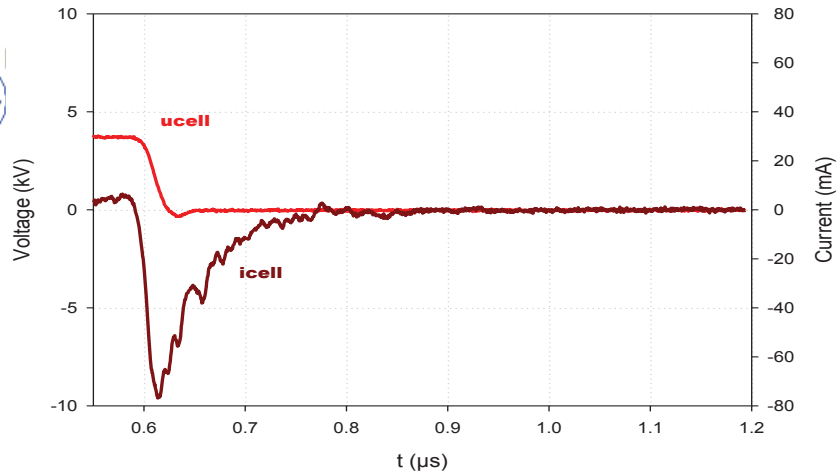
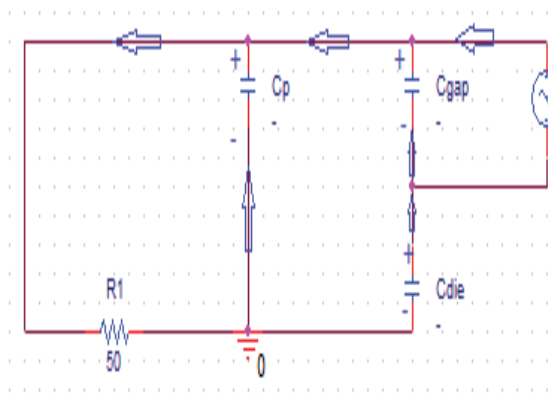
1 on 2 off (with discharge)



1 off 2 on (without discharge)



1 off 2 on (with discharge)



Voltage and current wave forms

Typical measured driving voltage u_{cell} and cell current i_{cell} are depicted in Fig. 18 in the pulse voltage we can verify that in the same period i_{cell} present two peaks one positive and other negative.

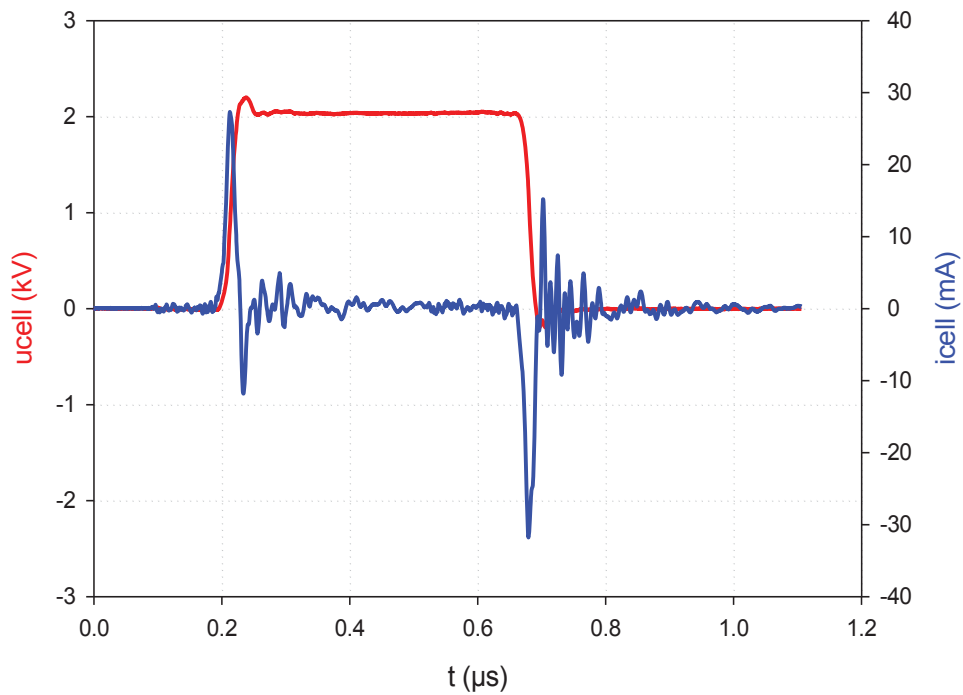


Fig 22: $P=100T, d=2mm$

For the all xenon pressures and all distance, waves forms of the cell current were quite similar, differing only by the values of their rise times, pulse durations, and maximum value of the discharge.

Characteristic of the microdischarge

The Fig. 23 shows the behavior of the microdischarge.

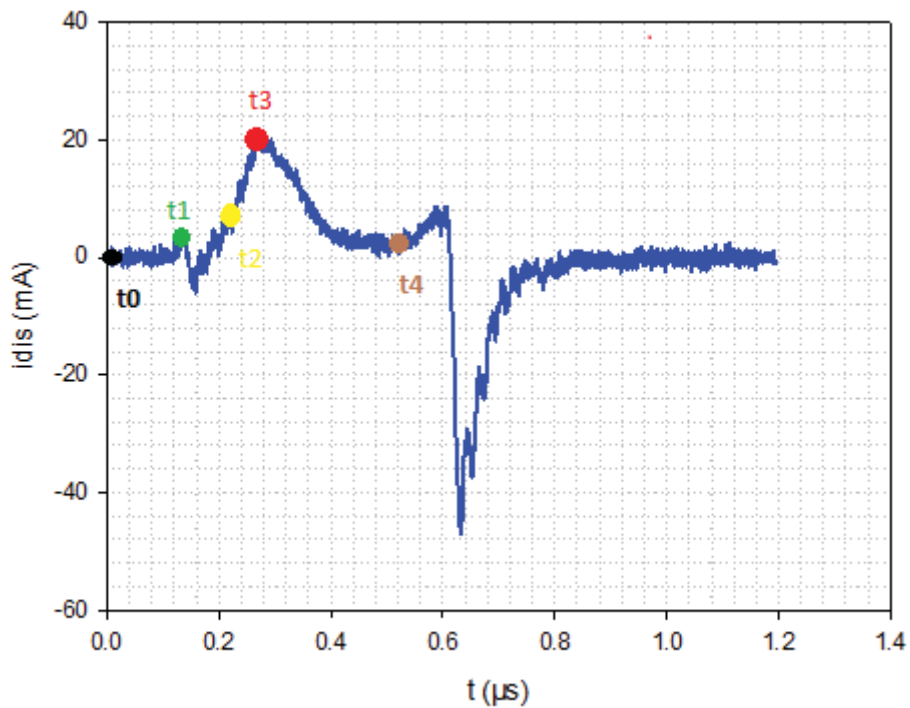
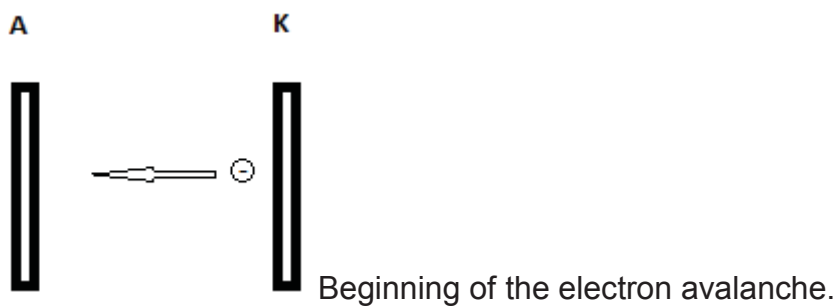
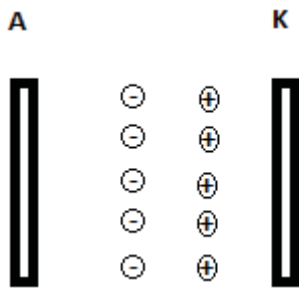


Fig 23: $P=400\text{Tor}$, $d=2\text{mm}$

t=0

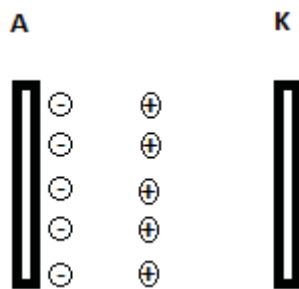


$t_0 < t < t_1$



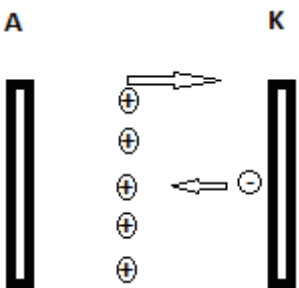
The electrons, which move faster than protons, go in the anode direction.

$t = t_1$



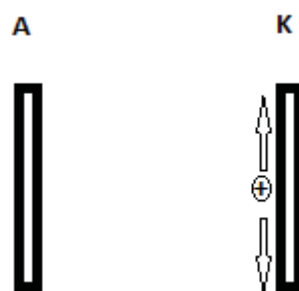
When the ionization wave hits the anode the charge are deposited on the surface of the anode, causing a local reduction of the axial electric field. In this instant the current decreases.

$t_1 < t < t_2$



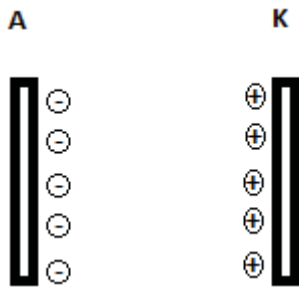
Beginning of the second avalanche, the electrons go in the direction of the proton barrier moving the protons to the cathode. During this process we check an increase considered current i_{dis} .

$t > t_2$



The protons tend to occupy the entire area of the cathode wall.

t=t3



The current increases until reaches its maximum (t=t3). The charges which accumulate on dielectric surfaces induce an electric field that opposes the applied field. The axial electric field in the gas tends to decrease, this leads to a decreases the speed of current rise.

t>t4

We can't analyze in detail this zone, is necessary better measurement equipment.

DBD-establishmentfor3 mm gap at 400 Torr

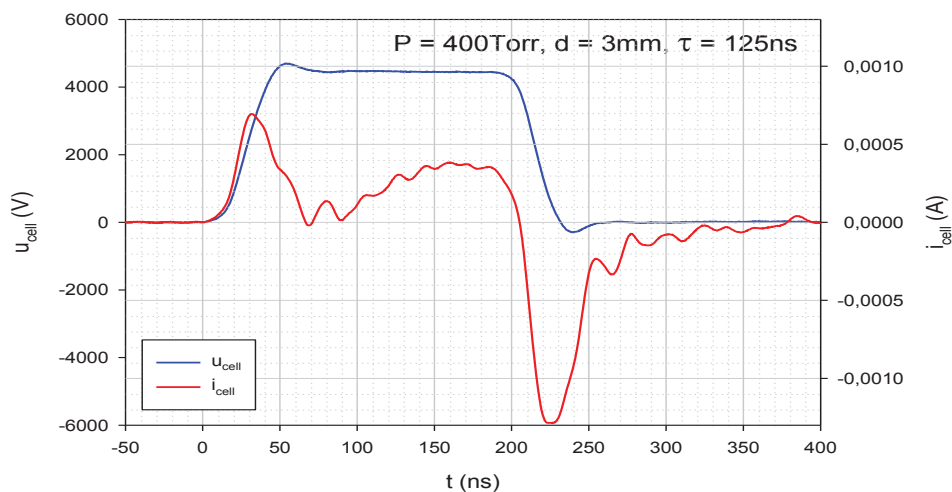


Fig. 24 : u_{cell} , i_{cell} and i_{cell_disp} for the MF-DBD:
 $P_{Xe} = 400 \text{ Torr}$, $d = 3 \text{ mm}$, $p.r.r = 9.705 \text{ kHz}$, $\tau = 125 \text{ ns}$.
 Reference: Laboratory LAPLACE

Here we will first discuss the results obtained at 400 Torr and $d = 2.5 \text{ mm}$, for which the supply current i_{cell} is less influenced by some fast oscillations (fig. 1):

$$V = (4309 \pm 15) \text{ V}, \tau = (151 \pm 1) \text{ ns}, t_{vr} = (24.9 \pm 0.2) \text{ ns}, t_{vr} = (20.3 \pm 0.2) \text{ ns}.$$

The supply current is constituted of three pulses: the 1st and 3rd ones are sharp (~60 ns duration) and fast rising (~15 ns). The displacement i_{cell_disp} flowing through $C_p // C_{cell}$ (respectively the stray and cell capacitors) is systematically recorded in the absence of any discharge, but with all other experimental conditions kept

unchanged. Our measures (not given) show that the 1^{st} and 3^{rd} pulses are mainly due to i_{cell_disp} that mask any discharge current.

The 2^{nd} current pulse is slower and longer. It is undoubtedly linked to a discharge, because the supply voltage hardly varies during this phase.

The snapshots of figures 2, 3 & 4 illustrate 5 discharge phases. Time origin ($t = 0$ ns) is the beginning of the supply voltage pulse. The 1^{st} discharge is an electronic avalanche (fig. 25) starting when the gap voltage attains the ignition voltage. It rapidly propagates towards the anode (A) during ~ 12 ns with a typical funnel-shape expansion. It is masked by i_{cell_disp} .

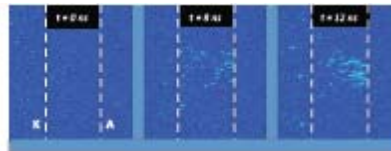


Fig.25: Spatio-temporal evolution of the electronic avalanche at 400 Torr, and 3mm gap.
Reference: Laboratory LAPLACE

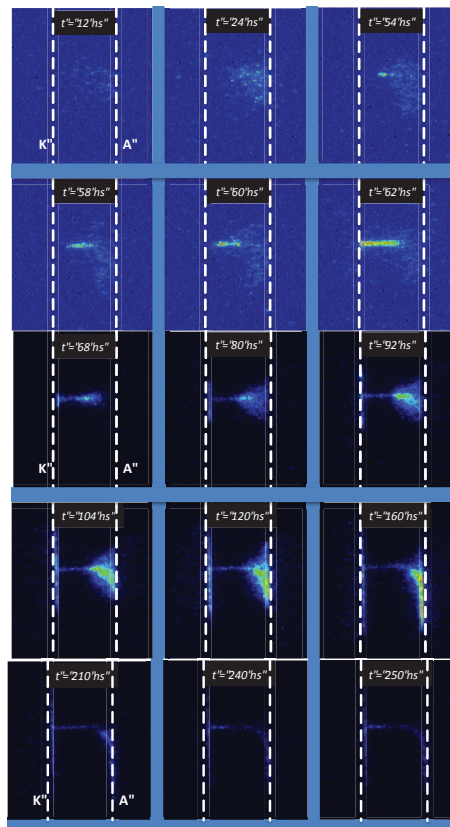


Fig. 26: Spatio-temporal evolution of the 1^{st} streamer and the 1^{st} cathode layer, at 400 Torr and 3 mm gap.
Reference: Laboratory LAPLACE

In fig. 26, a cathode-directed ionisation wave can be seen. Contrary to the sine-mode [15], this 1^{st} streamer takes ~ 42 ns to grow up before accelerating during the last ~ 8 ns. It reaches the electrode at ~ 62 ns.

Then it follows a 1^{st} cathode layer (fig. 26). Its radial cross-section increases, thus leading to the current raise. Meanwhile the charges deposited on the electrodes weaken the axial electric field, and subsequently i_{cell} . The last three snapshots

(fig.26) suggest that the discharge current i_{dis} should vanish out. However, in fig.24 this phenomenon is masked by the $i_{\text{cell disp}}$.

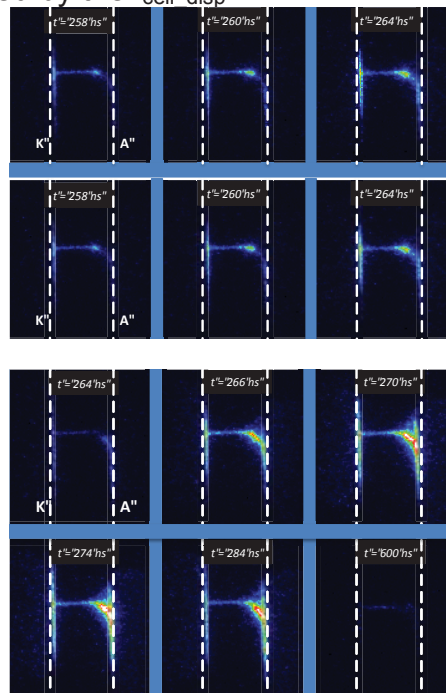


Fig. 25: Spatio-temporal evolution for 400 Torr and 3 mm. (a) Between 258 and 264 ns: 2nd streamer. (b) Between 264 and 600 ns: 2nd cathode layer. Reference: Laboratory LAPLACE

Just following the voltage pulse, a new discharge propagates towards the left electrode A (fig. 25). In fact, even if the applied voltage remains ~ 4.8 kV, once the 1st streamer is choked, no discharge can occur in the gap volume, unless a fast-falling voltage edge supervenes, for instance ~ 200 ns.

Due to the accumulated charge during the 1st cathode layer formation, the right electrode acts now as a virtual anode whereas the left one becomes a virtual cathode. During the falling edge of the voltage pulse, a high axial negative electric field appears in the gap, and accelerates secondary electrons from the virtual cathode to induce a 2nd streamer propagating towards the virtual anode K within 6 ns, faster than the 1st streamer. Then, a 2nd cathode layer occurs at the virtual cathode K. It grows much faster than the 1st one.

Temporal evolution of current

The three currents i_{cell} , i_{cellD} , i_{cell_dis} , are given in the Fig. 26. We can see the first and the second streamer, with the change of direction of the current.

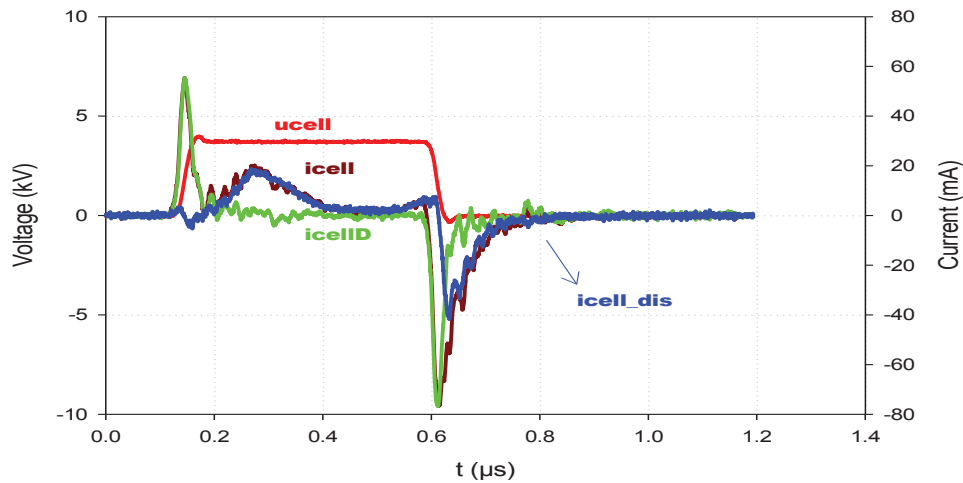


Fig 26: $P=400\text{Tor}$, $d=2\text{mm}$

Energy into one microdischarge

The energy into one microdischarge is depicted in Fig. 21.

In the first streamer the capacitor stores energy $u_{dis}>0$, $i_{dis}>0 \Rightarrow P_{dis}>0$

In the second streamer $u_{dis}<0$, $i_{dis}<0 \Rightarrow P_{dis}>0$

In the graphic is possible check the increase of E_{dis} .

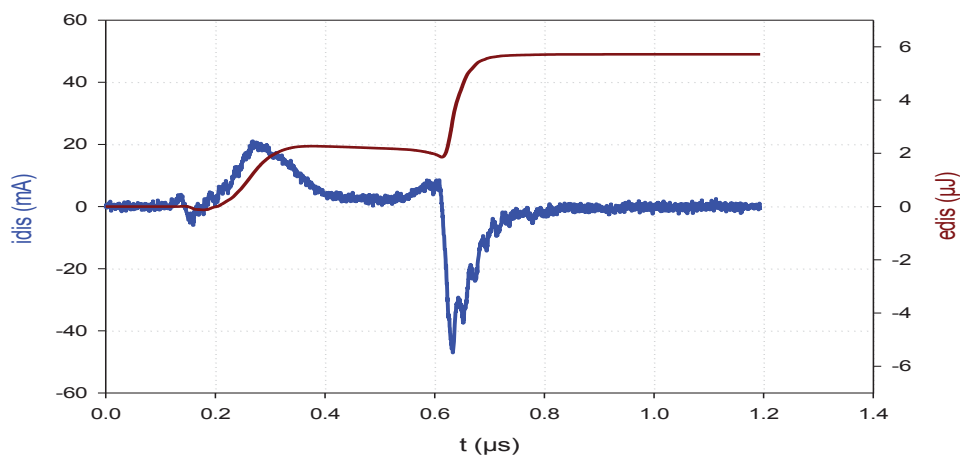


Fig 27: $P=400\text{ Torr}$, $d=2\text{mm}$

Pressure influence

A low pressure (100T 200T) the pressure influence is negligible, but as we increase the pressure the increase of the energy is more appreciable.

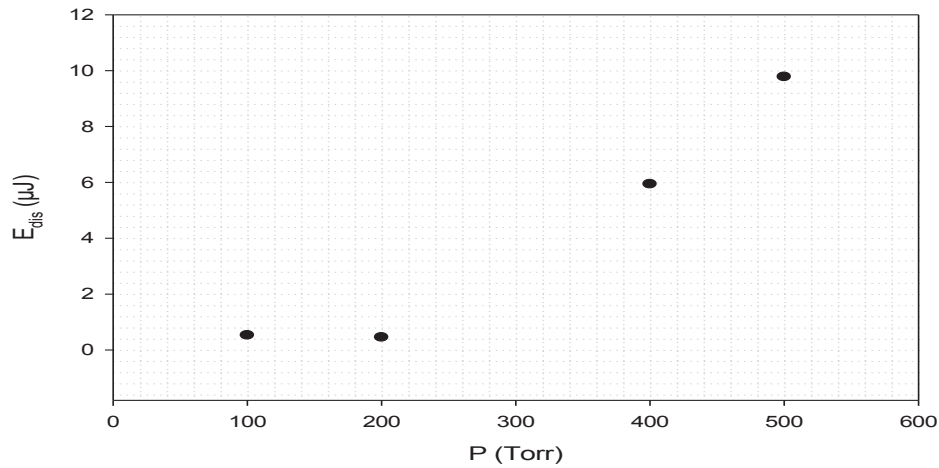


Fig 28: P variable, $d=2mm$, $f=9.69 Hz$

Distance influence

The energy into one microdischarge increases with the increase of the distance, such behavior can be verified in the following Fig. 28.

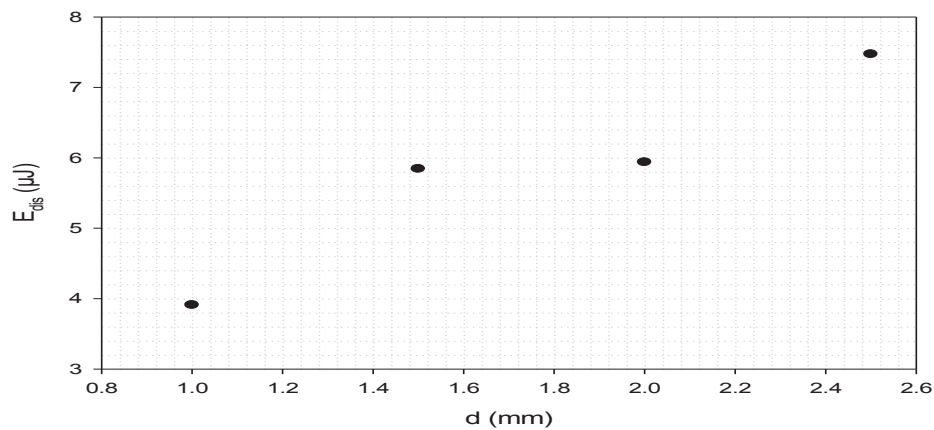


Fig. 28: $P=400 Torr$, $f=9.69 kHz$, $d=1, 1.5, 2, 2.5 mm$

Ignition voltage

Pressure influence

The pressure is directly proportional to the ignition voltage.

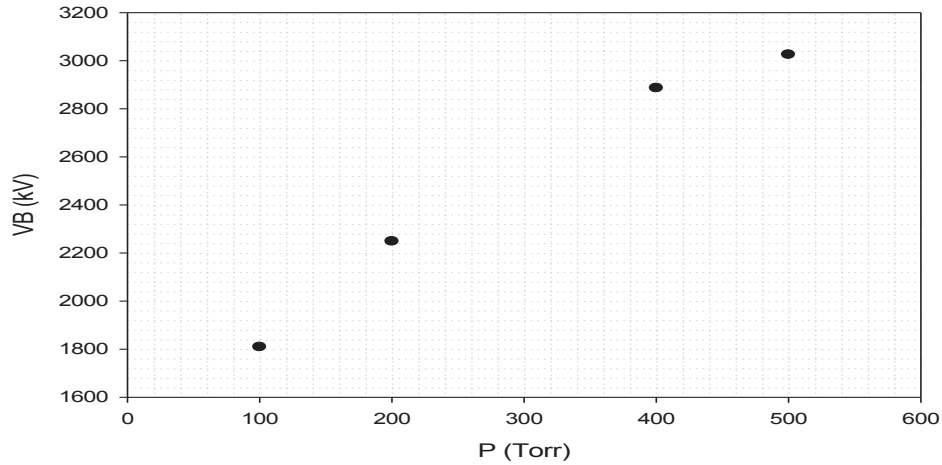


Fig. 29: P variable, $d=2\text{mm}$, $f=9.69\text{ Hz}$

Distance influence

As was expected with greater distance greater voltage necessary to beginning the microdischarge.

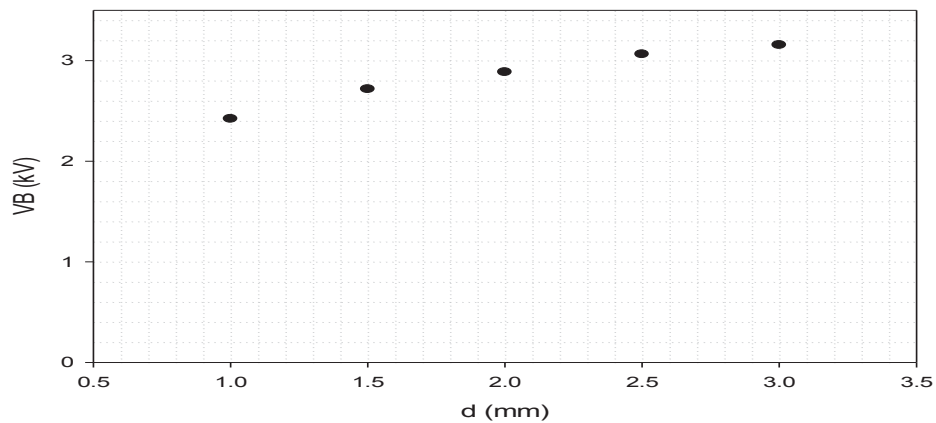


Fig. 30: $P=400\text{ Torr}$, $f=9.69\text{ kHz}$, $d=1, 1.5, 2, 2.5\text{ mm}$

Matlab

To calculate the principal value of the microdischarge the software Matlab is very important.

Objective:

1. Calculation of capacitor C_p
2. Results file
3. Simulation of idis

Operating description

1. Is necessary import all experimental measures to the Matlab language.
2. It manipulates the graphics to get the points of the easiest way.
3. Using the equations listed above and some points calculated graphically is possible to obtain the main characteristics of the microdischarge.
4. Interpretation of results

Difficulties

1. Nonlinear behavior
2. U_{cell} derivate
3. Manipulates the graphics

Interpretation of results

Calculation of capacitor C_p

	100T	200T	400T	500T
$C_{p_mont_moy}(pF)=$	0.2347	0.2328	0.3291	0.3304
$C_{p_desc_moy}(pF)=$	0.2542	0.2432	0.4639	0.3420
$C_{p_montD_moy}(pF)=$	0.2185	0.2331	0.3294	0.3263
$C_{p_descD_moy}(pF)=$	0.2287	0.2304	0.3665	0.3337

The capacitor with discharge and without has approximately the same capacitance value. So we can say that the capacitor has a linear behavior.

Voltage rise time

	100T	200T	400T	500T
t _{rise_monte_u} cell(ns)	18.55	19.6	26.6	26.7
t _{rise_do_u} cell(ns)	21.2	24	26.4	26
	1mm	1.5mm	2mm	2.5mm
t _{rise_monte_u} cell(ns)	18.55	19.6	26.6	26.7
t _{rise_do_u} cell(ns)	21.2	24	26.4	26
VB (V)	1809.6269	2249.2426	2886.8514	3051.9907

Considering: $i_{cell} = C_{total} * \left(\frac{dU_{cell}}{dt}\right)$

1. When the rise time increases the i_{cell} value decreases
2. When V_B increases i_{cell} increases

In the Fig.31 you can see that the VB influence is more important.

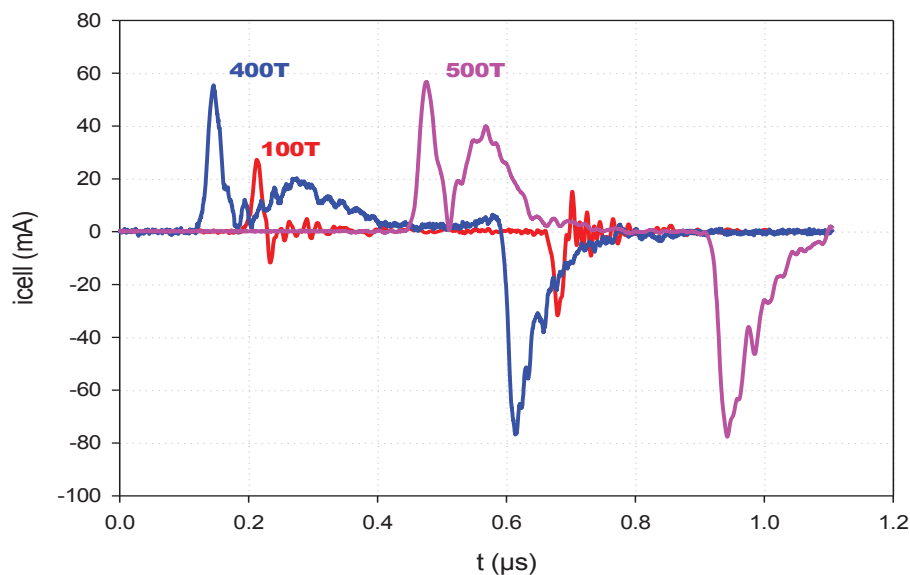


Fig. 31: $d=2mm$, $f=9.69$ Hz, $P=100, 400, 500$ Torr

The rise time increase when increase the pressure this should result in a decrease of i_{cell} but the influence of VB is most important this makes that grow i_{cell} .

Application

Ethylene elimination.

A industrial application for this study is the ethylene elimination. This is very important to the food industry, more exactly in time to transport and store.

In its natural state, the fruit emits ethylene to the environment. The ethylene is a natural ripening hormone. The Fig () shows the cycle of the ethylene production that accelerate of ripening processes.

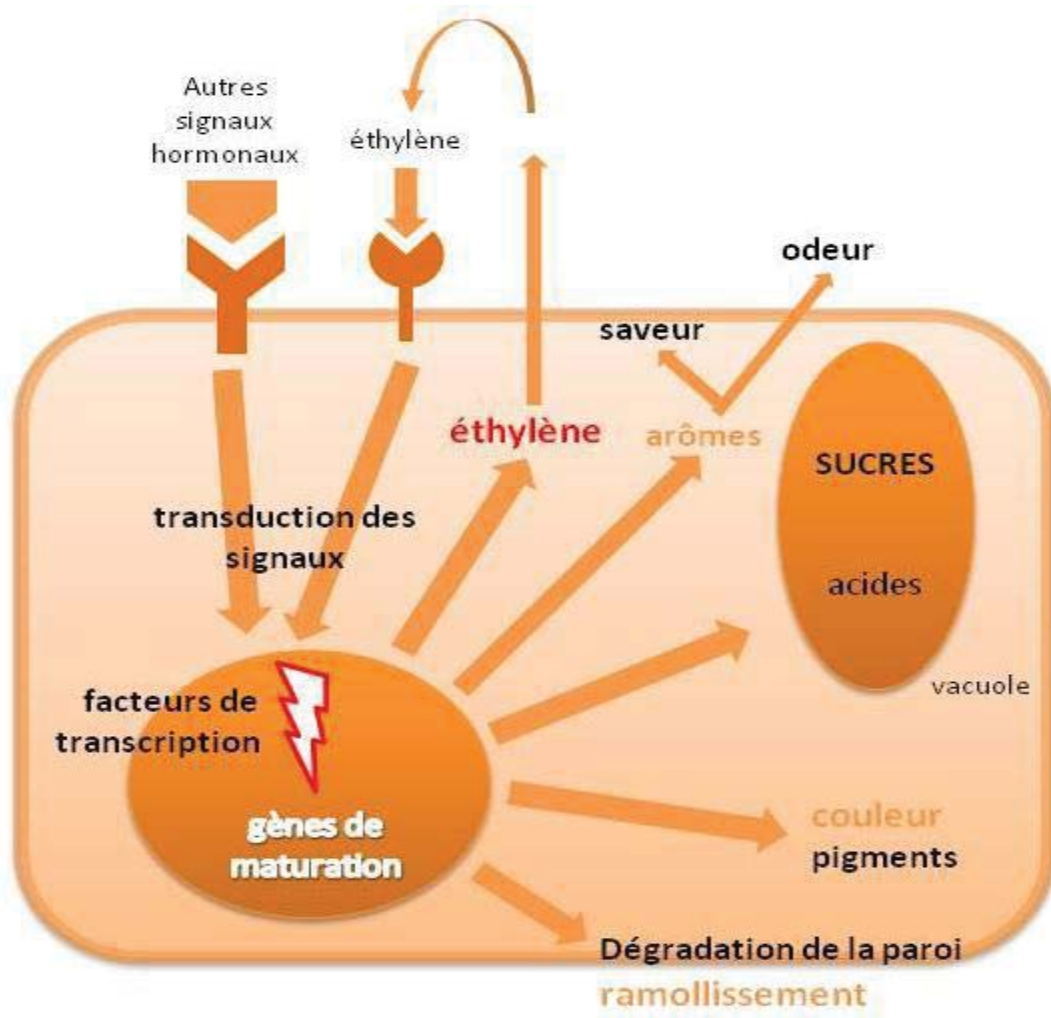


Fig. 32: Simulation of the accelerate of the ripening processes.

Reference: Présentation Claire Lafossas 04/06/2013

So to preserve the fruit for longer is necessary to eliminate the ethylene gas emitted by them. To remove the gas is used a new photocatalytic process, developed by the chemistry lab together the lab LAPLACE.

New photocatalytic process

Experimental Setup

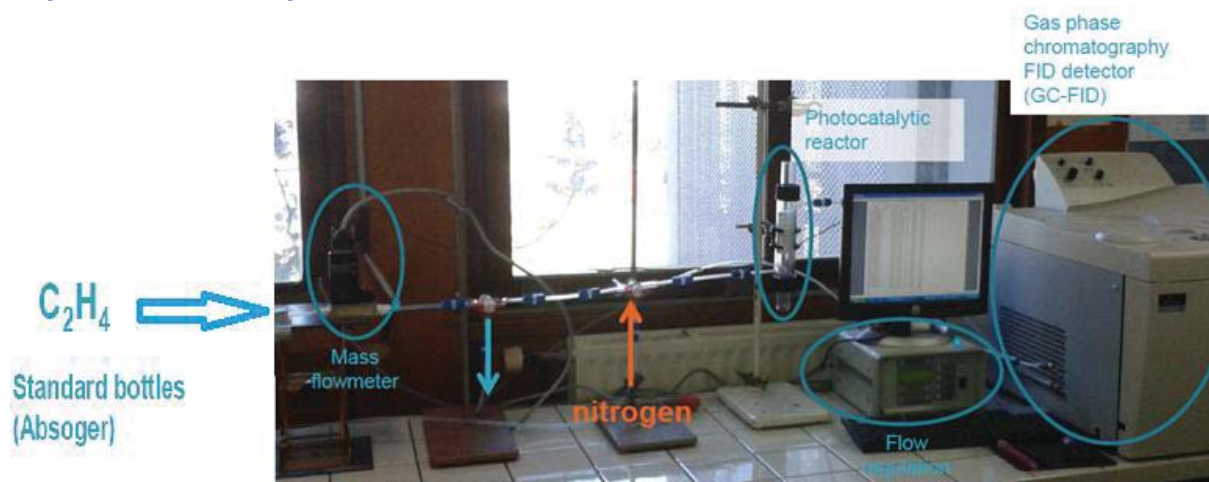


Fig. 32: Experimental Setup

Reference: Présentation Claire Lafossas 04/06/2013

Operating description of the photocatalytic reactor

1. There is a continuous flow of water which prevents overheating.
2. We introduce a flow, regulated, of ethylene in the photocatalytic reactor.
3. When the concentration of ethylene is almost 99% we turn on the lamp.
4. Is generated numerous discharge that generate vuv radiation.
5. The vuv radiation exited the TiO_2 that reacted with ethylene (C_2H_4).

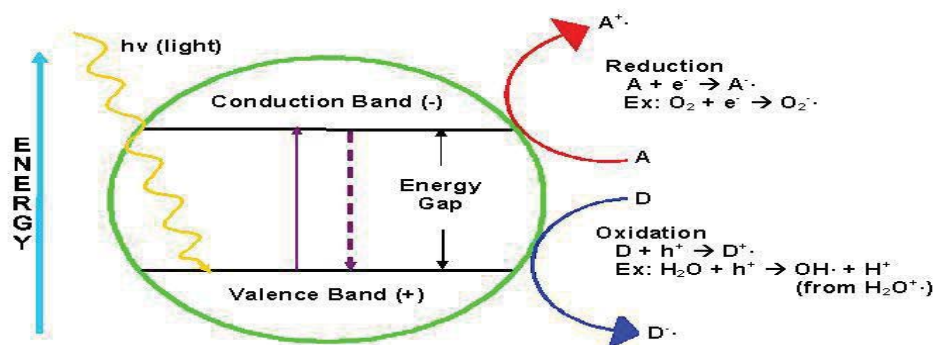


Fig. 33: Simulate of the reaction

Reference: Présentation Claire Lafossas 04/06/2013

6. The TiO_2 reacts with the ethylene that is decomposed as follows:



Conclusion

The present electrical analysis indicates that xenon and air synthetic microdischarges have many similarities.

It is possible, too, to verify the different behavior of the microdischarges generated with sinusoidal and pulse voltage.

Xenon mono-filamentary DBDs achieved with a mono-polar pulsed voltage show five different discharge phases: fast electronic avalanche, followed by a cathode directed streamer and the subsequent cathode layer, a more intense and faster streamer and its subsequent fast virtual cathode layer. Their individual speeds are estimated. The propagation speed of both streamers increases with increasing pressure and gap distance.

The study of the dielectric barrier discharges important to know what the best pressure, distance, gas, frequency, source voltage to use in which application, on this way we can save energy and consequently save money.

This study can be improved with better measurement equipment.

Bibliography

Nofel Merbahi Thèse de l'université Paul Sabatier N° 8 Toulouse France

N. Merbahi, G. Ledru, N. Sewraj and F. Marchal 2007 J. Phys. D. : Appl. Phys. **101** 123309

N Merbahi, N Sewraj, F Marchal, Y Salamero and P Millet 2004 J. Phys. D. : Appl. Phys. 1664–1678

N Sewraj, N Merbahi, F Marchal, G Ledru and J P Gardou 2009 J. Phys. D. : Appl. Phys. **42** 045206

N Sewraj, N Merbahi, J P Gardou, P Rodriguez Akerreta and F Marchal 2011 J. Phys. D. : Appl. Phys. **44** 145201

E. Leysenne, N. Sewraj, N. Merbahi, F. Marchal, M. C. Bordage 2013 , N° 10 LAPLACE